ELSEVIER

Journal of Power Sources 63 (1996) 209–214

JOURNAL OF POWER SOURCES

Discharge behaviour of Mg_2Ni-type hydrogen-storage alloy electrodes in 6 M KOH solution by electrochemical impedance spectroscopy

N. Cui, B. Luan, H.K. Liu, S.X. Dou

Institute for Materials Technology and Manufacturing, University of Wollongong, Northfields Avenue, Wollongong, NSW 2522, Australia

Received 1 July 1996; accepted 20 September 1996

Abstract

The discharge behaviour of Mg_2Ni-type hydrogen-storage alloy electrodes in 6 M KOH is investigated by a.c. impedance at room temperature. Comparative measurements are also performed on an $LaNi_5$ electrode. The rate-determining step of the discharge process for the magnesium-based hydrogen-storage alloy electrode is dependent on the alloy composition and depth-of-discharge. The unmodified Mg_2Ni has a high charge-transfer and mass-transfer resistance compared with $LaNi_5$. Additions of yttrium and aluminium in Mg_2Ni reduced considerably both the resistances and, thereby, produce a remarkable improvement in discharge capacity and rate-dischargeability.

Keywords: Magnesium alloys; Yttrium; Aluminium; Hydrogen-storage alloys; Electrochemical impedance spectroscopy

1. Introduction

Although many studies have been made [1–11] of the ability of magnesium-based alloys to absorb hydrogen in the gas phase, very few investigations have dealt with the electrochemical properties of these systems. More recently, it has been found [12–14] that modified Mg_2Ni-type alloy can undergo hydriding/de-hydriding in an alkaline solution at ambient temperature. The electrochemical capacity of this alloy is still less than that of $LaNi_5$ and Ti_2Ni alloys, although the gaseous capacity of the former is much more than that of the latter [15–20]. In addition, the rate-dischargeability of magnesium-based alloys is unsatisfactory.

Electrochemical impedance spectroscopy (EIS) is a powerful method for understanding interface processes and electrode behaviour [21–23]. Recently, Kuriyama et al. [24–26] applied EIS to characterize Mm-based alloy hydride electrodes and to study the deterioration behaviour of these electrodes. They proposed [26] that the deterioration of a metal-hydride electrode using copper-coated alloy powder was caused by passivation of the alloy surface only, while the performance of an electrode using uncoated alloy was dominated by an increase in the contact resistance.

In a previous paper [13], we reported that the electrochemical capacity and the rate capacity of Mg_2Ni alloy in 6 M KOH solution were considerably improved by the addition of yttrium and aluminium. The purpose of this work is to study the electrochemical behaviour of Mg_2Ni-type alloy electrodes by using EIS, and compare this behaviour with that of $LaNi_5$ alloy electrodes.

PII S0378-7753(96)02473-1

2. Experimental

2.1. Alloy preparation

Mg_2Ni and $Mg_{1.9}Al_{0.1}Ni_{0.9}Y_{0.1}$ alloys were prepared by the conventional powder metallurgical technique described previously [12,13]. The $LaNi_5$ alloy was made using a vacuum arc furnace under argon protection. The buttons were turned over and remelted for several times to ensure homogeneity. Subsequently, the obtained $LaNi_5$ buttons were annealed for five days in argon atmosphere at 1050 °C.

2.2. Electrode fabrication

The alloy buttons were mechanically ground to powders. After pulverisation, the sieved alloy powders of less than 400 mesh were mixed with 20 wt.% TAB-3 (Teflon acetylene black composite binder). The electrodes were fabricated by pressing this powder mixture onto both sides of a foam nickel sheet (2 cm × 3.5 cm) that was connected to a nickel wire by spot welding.

2.3. Charge/discharge procedures

Charge/discharge cycles were carried out at ambient temperature by using an automatic galvanostatic charge/dis-

charge controller (DEC-1). The test data were recorded by a Macintosh computer with a MacLab/8 analog/digital interface. The electrodes were charged to gassing voltage, rested for 30 min, and then discharged galvanostatically to −0.50 V versus a Hg/HgO reference electrode.

2.4. Electrochemical measurements

The electrochemical measurements were performed in a double compartment cell in which the hydrogen-storage alloy working electrode was separated from the counter electrode by a porous frit. A foam nickel sheet (7 cm × 20 mm) was used as a counter electrode and a Hg/HgO electrode as a reference electrode. The electrolyte used was 6 M KOH solution. The electrochemical impedance spectra were measured using an EG&G Princeton Applied Research electrochemical impedance analyser Model 6310 driven by a Model 398 electrochemical impedance software (v.1.23) with an IBM-PC 486 computer. The a.c. amplitude was 5 mV, and frequency range studied was between 5 mHz and 5 kHz. The impedance measurements were conducted at different depths-of-discharge (DOD) and at ambient temperature.

3. Results and discussion

3.1. Charge/discharge characteristics

The comparison of electrode charge/discharge characteristics for Mg_2Ni-type alloys, and an $LaNi_5$ alloy is given in Table 1. The discharge capacity of unmodified Mg_2Ni alloy electrode is only 8 mAh g^{-1} which is almost negligible compared with its theoretically electrochemical capacity [12]. The aluminium and yttrium additive Mg_2Ni-type alloy, $Mg_{1.9}Al_{0.1}Ni_{0.9}Y_{0.1}$, however, has a much higher discharge capacity, viz., 150 mAh g^{-1}. This indicates that the electrode behaviour of the Mg_2Ni alloy electrode is improved significantly by the substitution of alloy elements. The reasons for this have been subjected to a preliminary investigation by a linear polarization technique [13]. Although the rate-dischargeability of magnesium-based alloys is effectively improved by the addition of aluminium and yttrium, it is still much lower than that of $LaNi_5$ and Ti_2Ni alloys. In order to understand the de-hydriding kinetics of magnesium-based alloys in an alkaline solution and the effects of aluminium and yttrium additives on the electrochemical behaviour, the EIS of magnesium-based alloy electrodes have been measured. The EIS results for these electrodes are compared with those of $LaNi_5$ electrode.

Table 1
Comparison of electrode characteristics

Alloy	Discharge capacity		Rate-dischargeability C_{20}/C_5 (%)
	C_5 [a] (mAh g^{-1})	C_{20} [a] (mAh g^{-1}) [a]	
Mg_2Ni	8		
$Mg_{1.9}Al_{0.1}Ni_{0.9}Y_{0.1}$	150	104	69
Ti_2Ni	171	163	95
$LaNi_5$	336	327	97

[a] C_n refers to the discharge capacity at a discharge current density of n mA g^{-1}.

3.2. Electrochemical impedance spectra

In alkaline solutions, the overall reactions of hydrogen-storage alloy electrodes during charge and discharge are as follows:

(i) solid–liquid interface reaction

$$H_2O + M + e^- \underset{\leftarrow \text{discharge}}{\overset{\text{charge}\rightarrow}{\Leftrightarrow}} MH_{ad} + OH^- \quad (1)$$

(ii) solid-state reaction

$$MH_{ad} \underset{\leftarrow \text{discharge}}{\overset{\text{charge}\rightarrow}{\Leftrightarrow}} MH_{lattice} \quad (2)$$

When charging, hydrogen is generated by electrolyzing water according to reaction (1), and absorbs at the electrode surface in a highly active atomic state. Then, it diffuses into the lattice positions of metal phases to form a metal hydride as expressed by reaction (2). During discharging, the atomic hydrogen diffuses from the lattice position in the alloy to the metal/electrolyte interface. The hydrogen atom is oxidized at this interface. It should be noted that atomic hydrogen is supplied directly by electrolyzing on the electrode surface, rather than dissociating into hydrogen atoms from hydrogen molecule as hydriding in gaseous phase.

Typical Nyquist, Bode-modulus and Bode-phase plots for an Mg_2Ni electrode for various DODs at room temperature are shown in Figs. 1–3, respectively. As seen in the Nyquist plot (Fig. 1), the loci are composed of a distorted capacitive semi-circular arc at high frequencies and a midly curved line at low frequencies. The former is considered to be due to a

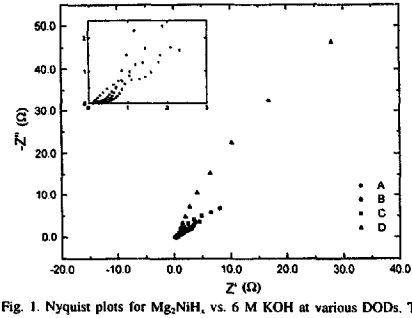

Fig. 1. Nyquist plots for Mg_2NiH_x vs. 6 M KOH at various DODs. The figure inset on the left-above is a magnified plot for the high-frequency data. A: 5% DOD; B: 20% DOD; C: 70% DOD, and D: 90% DOD.

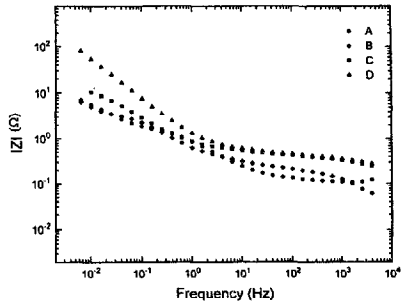

Fig. 2. Bode-modulus plots for Mg_2NiH_x vs. 6 M KOH at various DODs. A: 5% DOD; B: 20% DOD; C: 70% DOD, and D: 90% DOD.

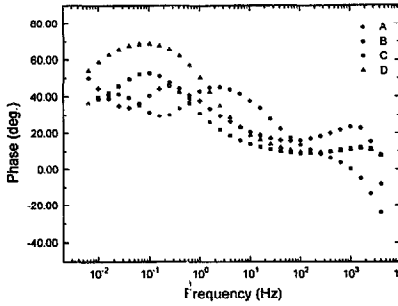

Fig. 3. Bode-phase plots for Mg_2NiH_x vs. 6 M KOH at various DODs. A: 5% DOD; B: 20% DOD; C: 70% DOD, and D: 90% DOD.

charge-transfer process at the electrode/electrolyte interface, as shown in Eq. (1), while the latter results from mass-transfer effects and is called the Warburg impedance. For the hydriding/de-hydriding reaction in an alkaline solution, the mass-transfer process generally includes the diffusion of H, OH^- and H_2O. Because the diffusivity of OH^- and H_2O in the alkaline solution is much larger than that of hydrogen atoms in the solid phases (hydrides, alloys or oxides), the diffusion of hydrogen atoms in solid phases is considered to be mainly responsible for the mass-transfer effects of the metal-hydride electrodes.

The impedance analysis was carried out by using the Randles–Ershler equivalent circuit model (Fig. 4), in which an

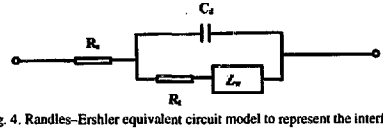

Fig. 4. Randles–Ershler equivalent circuit model to represent the interfacial impedance for dehydriding reaction of the hydrogen-storage alloy electrode in 6 M KOH solution.

ohmic resistance, R_s, is in series with a parallel combination of the double-layer capacitance, C_d, and the charge-transfer resistance, R_t, which is a series combination of the Warburg impedance Z_w. As found in Fig. 1, an increase in R_s with increasing DOD is displayed by the Mg_2Ni hydride electrode. It is believed that this behaviour is associated with the formation and growth of the oxide and/or layer on the alloy surface.

Analysis of the EIS data (Figs. 1–3) reveals that the electrode kinetics change with DOD. At the initial stage of discharge (DOD = 5%), as seen on the locus A in Fig. 1, both a partially resolved semi-circle locus at high frequencies and a linear impedance locus at low frequencies are observed, and neither of them is negligible. This indicates that the discharging process of the Mg_2Ni hydride electrode is dictated by both the charge-transfer process at the electrode/electrolyte interface and the diffusion of hydrogen atoms in the alloy. The Warburg impedance region (originating from atomic hydrogen diffusion in the electrode) increases appreciably with increasing DOD. This is due to the fact that the concentration of hydrogen in the metal-hydride electrodes decreases with increase in the DOD, and lower concentrations could increase the mass-transfer impedance [27]. When the DOD increases to or beyond 70%, the absence of a semi-circle in the complex-plane reveals a fast charge-transfer process and slow diffusion for hydrogen in the alloy at this stage. Thus, the controlling-step of the discharge process for an Mg_2Ni electrode changes with DOD, from a mixed rate-determining process at the initial discharging stage to the hydrogen diffusion-controlled reaction at the final discharging stage.

The dependence of the modulus and the phase, versus frequency for Mg_2Ni are shown in Figs. 2 and 3, respectively. The modulus increases with increasing DOD in the measured frequency range, and decreases when the frequency is elevated at a given DOD. The phase angles in Fig. 3 seem to be associated with the frequency and DOD.

As is well known, $LaNi_5$ alloy has a very good electrochemical hydriding/de-hydriding performance when used as a metal-hydride electrode in alkaline solution. For the purposes of comparison, the EIS of an $LaNi_5$ electrode was measured at various DODs. The results are displayed in Figs. 5–7. At the initial stage of discharging (5% DOD), the loci A in Fig. 5 is composed of only a semi-circle arc, which differs from the locus A in Fig. 1 for Mg_2Ni. The linear region at low frequencies expressed as the Warburg impedance was not observed for $LaNi_5$ at 5% DOD. Therefore, the discharging process of the $LaNi_5$ hydride electrode is believed to be controlled by the charge transfer at the electrode/electrolyte interface at this stage. With increasing DOD, the semi-circle goes off into a Warburg region. This indicates that the Warburg impedance gradually dominates the discharging current. By a comparison of Fig. 2 with Fig. 6, it is noticed that at both the high-frequency end and the low-frequency end, the modulus of unmodified Mg_2Ni is one order of magnitude higher than that for $LaNi_5$ at all DODs. The values of modulus at high frequency for Mg_2Ni is high and dependent on DOD,

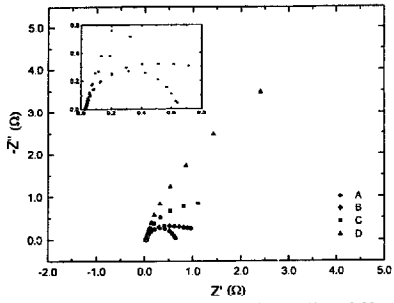

Fig. 5. Nyquist plots for $LaNi_5H_x$ vs. 6 M KOH at different DODs. The figure inset on the left-above is a magnified plot for the high-frequency data. A: 5% DOD; B: 20% DOD; C: 70% DOD, and D: 90% DOD.

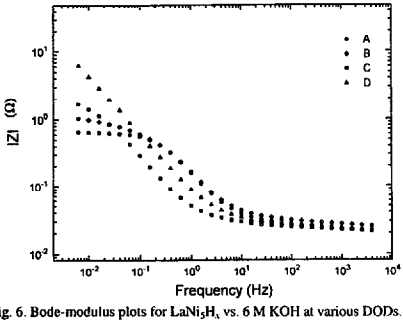

Fig. 6. Bode-modulus plots for $LaNi_5H_x$ vs. 6 M KOH at various DODs. A: 5% DOD; B: 20% DOD; C: 70% DOD, and D: 90% DOD.

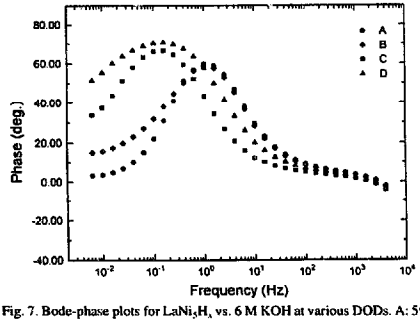

Fig. 7. Bode-phase plots for $LaNi_5H_x$ vs. 6 M KOH at various DODs. A: 5% DOD; B: 20% DOD; C: 70% DOD, and D: 90% DOD.

whilst $LaNi_5$ is not. This confirms the previous results that the oxide layer forms and grows on the Mg_2Ni surface with increasing DOD and, thereby, increases the electronic resistance. At low frequencies, however, it can be seen that the

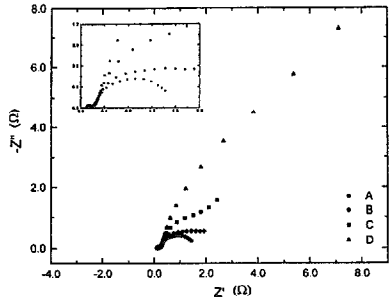

Fig. 8. Nyquist plots for $Mg_{1.9}Al_{0.1}Ni_{0.9}Y_{0.1}H_x$ vs. 6 M KOH at various DODs. The figure inset on the left-above is a magnified plot for the high-frequency data. A: 5% DOD; B: 20% DOD; C: 70% DOD, and D: 90% DOD.

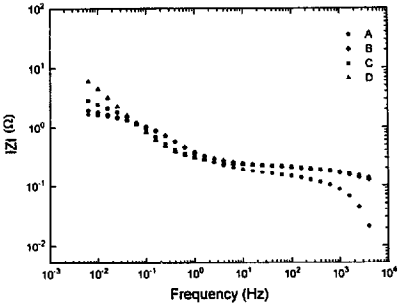

Fig. 9. Bode-modulus plots for $Mg_{1.9}Al_{0.1}Ni_{0.9}Y_{0.1}H_x$ vs. 6 M KOH at various DODs. A: 5% DOD; B: 20% DOD; C: 70% DOD, and D: 90% DOD.

modulus of Mg_2Ni, even at 5% DOD, is still larger than that of $LaNi_5$ at 90% DOD. These results explain why the Mg_2Ni electrode has a very low discharge capacity and sluggish kinetics.

The impedance spectra of the Mg_2Ni alloy modified by aluminium and yttrium additions are shown in Figs. 8–10. The results in Fig. 8 indicate that the ohmic resistance, R_s, for $Mg_{1.9}Al_{0.1}Ni_{0.9}Y_{0.1}$ is much smaller compared with that of Mg_2Ni, and R_s hardly changes with DOD. This suggests that the addition of aluminium in the alloy improves the passivating behaviour of the Mg_2Ni alloy, which is probably similar to that observed with Ti_2Ni systems as previously reported [17]. It can also be seen in Fig. 8 that, at the initial stage of discharging (5% DOD), the locus A is a semi-circle arc at all measured frequencies, a Warburg impedance region does not appear at low frequencies. This seems to be similar to that found with an $LaNi_5$ hydride electrode (Fig. 5). Consequently, for the $Mg_{1.9}Al_{0.1}Ni_{0.9}Y_{0.1}$ hydride electrode, the rate-determining step at 5% DOD is charge transfer at the electrode/electrolyte interface, rather than the mixed

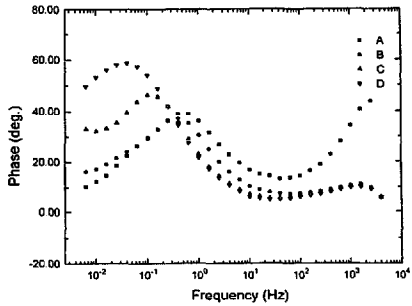

Fig. 10. Bode-phase plots for $Mg_{1.9}Al_{0.1}Ni_{0.9}Y_{0.1}H_x$ vs. 6 M KOH at various DODs. A: 5% DOD; B: 20% DOD; C: 70% DOD, and D: 90% DOD.

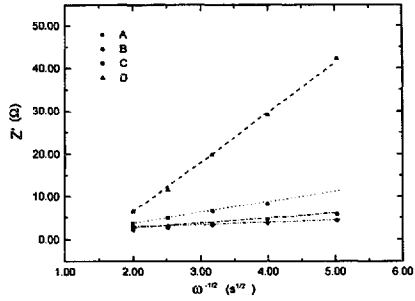

Fig. 11. Randles plots for Mg_2NiH_x vs. 6 M KOH at various DODs. A: 5% DOD; B: 20% DOD; C: 70% DOD, and D: 90% DOD.

rate-determining process witnessed with unmodified Mg_2Ni. At the various DOD, the modified Mg_2Ni displays a lower charge-transfer resistance and mass-transfer resistance than unmodified Mg_2Ni. These results demonstrate that the modified Mg_2Ni electrode has better electrochemical activity for hydrogen oxidization at the surface and faster hydrogen diffusion in the solid phases. Therefore, additions of aluminium and yttrium in Mg_2Ni result in a considerable increase in discharge capacity and rate-dischargeablity.

The effect of mass transfer is manifested through Warburg coefficient, σ. The Randles plots for various alloy hydride electrodes are shown in Figs. 11–13. These plots provide further evidence for a low-frequency Warburg response. The plots also show that the experimentally measured Warburg coefficient, $\sigma = dZ'/d\omega^{-1/2}$, is strongly dependent on the electrode materials and the DOD. The DOD dependence of the Warburg coefficient, σ, for various electrodes is given in Fig. 14. The values of σ at 90% DOD for unmodified Mg_2Ni (9.4 $\Omega\ s^{-1/2}$) and $LaNi_5$ (0.78 $\Omega\ s^{-1/2}$) differ by a factor of 12. This can be explained by the fact that the activation energy for hydrogen diffusion is 460 meV for Mg_2Ni and 275 meV for $LaNi_5$ [28,29]. The diffusion coefficient can be

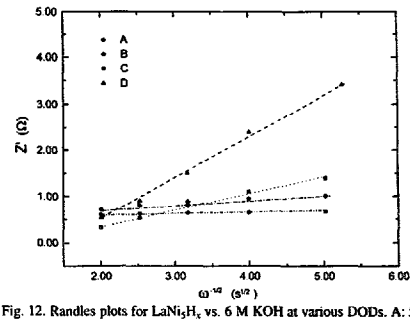

Fig. 12. Randles plots for $LaNi_5H_x$ vs. 6 M KOH at various DODs. A: 5% DOD; B, 20% DOD; C, 70% DOD; D, 90% DOD.

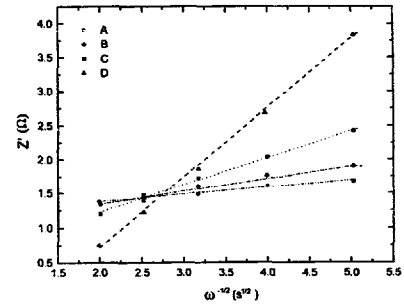

Fig. 13. Randles plots for $Mg_{1.9}Al_{0.1}Ni_{0.9}Y_{0.1}H_x$/6 M KOH at various DOD. A: 5% DOD; B: 20% DOD; C: 70% DOD, and D: 90% DOD.

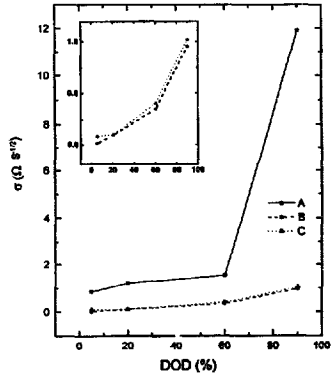

Fig. 14. DOD vs. Warburg coefficient, σ, for various alloys. A: Mg_2NiH_x; B: $LaNi_5H_x$, and C: $Mg_{1.9}Al_{0.1}Ni_{0.9}Y_{0.1}H_x$.

expressed as: $D = D_0 \exp(-E_a/RT)$, where E_a is the activation energy of the diffusion reaction, R is a gas constant, and T is the absolute temperature. Hence, the hydrogen diffusion in Mg_2Ni is expected to be slower than that in $LaNi_5$. Moreover, as mentioned above, a magnesium oxide and/or hydroxide layer forms and grows on the surface of the electrode with increase in DOD, which may also block hydrogen transfer from the bulk to the surface for discharging. Thus, the unmodified Mg_2Ni has a larger mass-transfer resistance than $LaNi_5$.

The results in Fig. 14 clearly show that an addition of aluminium and yttrium in Mg_2Ni decreases the value of σ. This is probably due to the fact that the substitution of yttrium for nickel in Mg_2Ni alloy causes an increase in the lattice constant (a, c) and the crystal cell volume [13], which is beneficial for hydrogen diffusion in the alloys. Furthermore, the addition of aluminium in the alloy is assumed to improve the passivating behaviour of the Mg_2Ni alloy. Thus, the formation and growth of the oxide film is limited, and the hydrogen migration resistance through this passivating layer is reduced. This is supported by the R_s data and the modulus data of $Mg_{1.9}Al_{0.1}Ni_{0.9}Y_{0.1}$ (see Figs. 8 and 9).

4. Conclusions

The discharge behaviour of Mg_2Ni-type hydrogen storage alloys in an alkaline solution at ambient temperature is investigated and compared with $LaNi_5$. EIS results indicate that the very low discharge capacity and sluggish kinetics of the unmodified Mg_2Ni electrode in alkaline solution are caused by the presence of both a larger charge-transfer resistance and a mass-transfer resistance. The formation and growth of a magnesium oxide and/or hydroxide layer on unmodified Mg_2Ni increase the electronic resistance at the electrode/electrolyte interface and result in a large discharging overpotential. The additions of yttrium and aluminium in Mg_2Ni considerably reduce the hydrogen-diffusion resistance in the alloy and the charge-transfer resistance on the electrode/electrolyte interface. As a result, the discharge capacity and rate-dischargeability of the electrodes are remarkably improved.

References

[1] J. Genossar and P.S. Rudman, *Z. Phys. Chem. N.F., 116* (1979) 215.
[2] A. Karty, J. Genossar and P.S. Rudman, *J. Appl. Phys., 50* (1979) 7200.
[3] M.E. Hammioui, L. Belkbir and N. Gerard, *J. Alloys Comp., 202* (1993) 199.
[4] J.J. Reilly and R.H. Wiswall, *Inorg. Chem., 7* (1968) 2254.
[5] H. Nagai, H. Tomizawa, T. Ogasawara and K. Shoji, *J. Less-Common Met., 157* (1992) 15.
[6] P. Mandal, K. Dutta, K. Ramakrishna, K. Sapru and O.N. Srivastava, *J. Alloys Comp., 184* (1992) 1.
[7] P. Mandal and O.N. Srivastava, *J. Alloys Comp., 205* (1994) 111.
[8] S. Orimo, H. Fujii and M. Tabata, *J. Alloys Comp., 210* (1994) 37.
[9] S. Orimo, M. Tabata and H. Fujii, *J. Alloys Comp., 203* (1994) 61.
[10] Zhou Ye, L.C. Erickson, B. Hjorvarsson, *J. Alloys Comp., 209* (1994) 117.
[11] K. Dutta and O.N. Srivastava, *Int. J. Hydrogen Energy, 18* (1993) 397.
[12] N. Cui, B. Luan, H.J. Zhao, H.K. Liu and S.X. Dou, *J. Power Sources, 55* (1995) 263.
[13] N. Cui, B. Luan, H.J. Zhao, H.K. Liu and S.X. Dou, *J. Alloys Comp., 233* (1996) 236.
[14] N. Cui, B. Luan, H.J. Zhao, H.K. Liu and S.X. Dou, *J. Alloys Comp., 240* (1996) 229.
[15] B. Luan, N. Cui, H.J. Zhao, H.K. Liu and S.X. Dou, *J. Power Sources, 55* (1995) 197.
[16] B. Luan, N. Cui, H.J. Zhao, H.K. Liu and S.X. Dou, *J. Power Sources, 55* (1995) 101.
[17] B. Luan, N. Cui, H.J. Zhao, H.K. Liu and S.X. Dou, *J. Alloys Comp., 233* (1996) 225.
[18] B. Luan, N. Cui, H.J. Zhao, H.K. Liu and S.X. Dou, *Int. J. Hydrogen Energy, 21* (1996) 373.
[19] B. Luan, N. Cui, H.J. Zhao, H.K. Liu and S.X. Dou, *J. Power Sources, 52* (1994) 295.
[20] F. Meli, A. Zuttel and L. Schlapbach, *J. Alloys Comp., 202* (1993) 81.
[21] J.R. Macdonald, *Impendance Spectroscopy*, Wiley, New York, 1987.
[22] P. Simon, N. Bui, N. Petere, F. Dabosi, J. Power Sources, *53* (1995) 163.
[23] M. Hughes, R.T. Barton, S.A.G.R. Karunathilaka, N.A. Hampon and R. Leek, *J. Appl. Electrochem., 15* (1985) 129.
[24] N. Kuriyama, T. Sakai, H. Miyamura, I. Uehara and H. Ishikawa, *J. Alloys Comp., 192* (1993) 161.
[25] N. Kuriyama, T. Sakai, H. Miyamura, I. Uehara and H. Ishikawa, *J. Alloys Comp., 202* (1993) 183.
[26] N. Kuriyama, T. Sakai, H. Miyamura, I. Uehara and H. Ishikawa, *J. Electrochem. Soc., 139* (1992) L72.
[27] A.J. Bard and L.R. Faulkner, *Electrochemical Methods Fundamentals and Applications*, Wiley, New York, 1980, p. 329.
[28] J.J.G. Willems and K.H.J. Buschow, *J. Less-Common Met., 129* (1987) 13.
[29] S.D. Goren and C. Korn, *J. Less-Common Met., 73* (1980) 261.